Kovove Mater. 61 2023 243–256
DOI: 10.31577/km.2023.4.243

Effect of graphene codeposition on tribological behavior of Ni-plated anodic hard coating

Maryam Bagheri, Behnam Lotfi*, Zohreh Sadeghian

Department of Materials Science and Engineering, Faculty of Engineering, Shahid Chamran University of Ahvaz, Ahvaz, Iran

Received 18 January 2023, received in revised form 18 April 2023, accepted 24 April 2023

Abstract

Graphene nanosheets and Ni were used to develop oxide matrix composite coating on anodic hard coating (AHC). Anodized Al-6061-T6 alloy was Ni plated in a solution containing 50 mg l^{-1} graphene nanosheets. The effect of plating time on the microstructure and properties of coatings was investigated. FE-SEM, EDS, and Raman spectroscopy were used to analyze the surface morphology, cross-section, and chemical composition of composite coatings. The presence of graphene seemed to result in the refinement of the Ni matrix grain structure. Vickers micro-hardness and dry sliding wear tests were conducted on the coatings. AHC + Ni/Gr showed 60 percent higher hardness than AHC + Ni coating (160 ± 34 HV). The presence of graphene in AHC + Ni/Gr coatings reduced the wear rate and average friction coefficient compared to AHC and AHC + Ni coatings. AHC + Ni/Gr obtained after 10 min electroplating presented the lowest wear rate. The dominant wear mechanism in AHC + Ni coating was fatigue wear, while AHC + Ni/Gr exhibited abrasion and delamination.

K e y w o r d s: anodic hard coating, nickel precipitates, graphene nanosheets, composite coating, friction coefficient

1. Introduction

Hard anodizing is a process widely used to improve the wear resistance of aluminum and its alloys. AHC film has a porous structure with high hardness and wear resistance as well as good corrosion resistance [1–5]. Moreover, hard anodized surfaces usually show relatively high friction coefficients when they slide against metallic counterparts. Filling the pores of the coating with lubricating materials like MoS_2, polytetrafluoroethylene (PTFE), and graphite has been suggested to reduce the friction coefficient [6–8]. Due to the deposition of a lubricating phase into the porosities of the anodic oxide film, the friction coefficient of the surface is effectively reduced, and a self-lubricating surface is obtained.

The application of composite layers containing AHC and different metals such as Ni, Cu, Cr, and Co is a new solution for the reduction of the friction coefficient and protection of components against drastic wear [9, 10]. Friction between sliding surfaces depends on the shear strength of the adhesion junction in the contact zone and the hardness of the material. Anodic oxide coatings provide high hardness, and the use of metal deposits provides low shear strength at junctions. Currently, AHC + metal coatings are applied to reduce the friction coefficient of a new engine under limited lubrication conditions [9]. AHC + Ni coating was first developed at the University of Silesia, Poland [11]. Nickel precipitates have plastic properties and reduce the friction coefficient. The friction of AlSi12-15%Al_2O_3 covered with AHC + Ni composite coating fabricated through the electroplating method was studied by Posmyk [12, 13]. It was suggested that the minimum time is required for the depositing of Ni precipitates upon the AHC coating surface (anodic oxide coating) when used with limited lubrication. The maximum time is the initial time when nickel precipitates merge into a continuous layer. This layer prevents the absorption of oil in the presence of lubrication, but in dry wear, it can create the desired conditions by ensuring the filling of a large percentage of

*Corresponding author: tel.: +98 611 3332739; e-mail address: behnaml@scu.ac.ir

pores and the covering of a large part of the anodic oxide coating.

Most metals or solid lubricants with low shear strength are relatively soft. Therefore, anodic oxide composites containing such materials may not attain high hardness values. Graphene, with a two-dimensional nanostructure, has attracted considerable attention as a lubricating nanomaterial due to its mechanical properties and low friction coefficient. The incorporation of graphene sheets into the nickel matrix through the electroplating method is currently used to improve the friction and wear resistance of nickel coatings [14–17]. Algul et al. [18] studied the effect of graphene content and sliding speed on the wear mechanism of nickel-graphene nanocomposites. They reported that increasing the graphene content of the electrolyte from 100 to 500 mg L^{-1} resulted in a significant increase in micro-hardness and wear resistance and a reduction in friction coefficient. In the present study, Ni and graphene nanosheets were codeposited on AHC through an electroplating process to improve its wear resistance and friction behavior. The effect of electroplating time on the structure and tribological behavior of coating has been investigated.

2. Experimental procedures

Samples made of AA6061 alloy with 50 mm × 50 mm × 2 mm dimensions were immersed in 10 wt.% NaOH aqueous solution at 50 ℃ for 5 min, then washed with deionized water. Next, the samples were immersed in 30 % HNO_3 aqueous solution for 1 min and rinsed with distilled water. Anodic oxidation was carried out in 15 wt.% H_2SO_4 solution using 16–40 V potential at –5 to –9 ℃ for 85 min. Subsequently, the anodized specimens were dipped in 5 vol.% phosphoric acid solution for 30 min to widen the pores and reduce the thickness of the oxide layer at the bottom of the pores.

AHC + Ni/Gr composite coatings were prepared through the electroplating of the specimens under AC current using a Watts bath. The bath solution was stirred using an ultrasonic probe with 200 W power for 20 min. Multilayer Gr nanosheets (3.7–5.5 nm thickness and 0.5–3 μm lateral dimension) were dispersed in the plating solution. Ultrasonic agitation and mechanical stirring were simultaneously used during the electroplating process. Ni plate of 99.9 % purity was used as the counter electrode, and electroplating was carried out at room temperature. The electroplating bath composition and process parameters are presented in Table 1. The samples denoted by AHC + Ni/Gr (10), AHC + Ni/Gr (15), and AHC + Ni/Gr (20) were prepared through electroplating for 10, 15, and 20 min, respectively. A pure Ni-plated sample was also prepared through electroplating for 20 min, for comparison. After electroplating, the coatings were washed and dried for further investigation.

Table 1. Bath compositions and electroplating conditions for AHC + Ni/Gr composite coating

$NiSO_4.6H_2O$	330 g l^{-1}
$NiCl_2.6H_2O$	30 g l^{-1}
H_3BO_3	30 g l^{-1}
SDS (Sodium dodecyl sulfate)	0.5 g l^{-1}
Graphene	50 mg l^{-1}
Temperature (℃)	Room temperature
Ph	5.5
Voltage	10 V
Anode	Nickel plate
Type of current	Alternating current (AC)
Time	10, 15, 20 min

Surface and cross-sectional morphologies of the coatings and wear tracks were studied using scanning electron microscopy (SEM) and field emission scanning electron microscopy (FE-SEM). Energy dispersive spectroscopy (EDS; Energy Dispersive X-Ray Spectroscopy) was used to analyze local composition on the surface of the coatings, wear tracks, and wear debris. Coatings were analyzed using Raman spectroscopy to determine the presence of graphene in the composite coatings. Micro-hardness of the coatings was measured using a Vickers hardness testing machine (Innova) under a 200 g load for 15 s dwell time. The average hardness value was obtained from 5 indentations on each sample.

Tribological properties of the coatings were investigated using pin-on-disk apparatus under unlubricated conditions. The tests were carried out at room temperature under a 10 N load and with a fixed rotating speed of 0.1 m s^{-1}. A 52100-steel pin of 5 mm diameter was used as the counter body.

3. Results and discussion

3.1. AHC microstructure

FE-SEM micrograph of the top surface of the AHC sample is illustrated in Fig. 1. As can be seen, the sample has a porous structure with an estimated average pore diameter of about 31 nm. It should be noted that pores larger than 50 nm deteriorate the tribological properties of AHCs as they cause a reduction in hardness. Therefore, coatings with a mean pore diameter of 15–50 nm are practically preferred [19].

FE-SEM micrographs of the cross-section and fracture surface of AHC are presented in Fig. 2. As can be observed in Fig. 2a, a uniform coating is of 50 μm thickness. There are some cavities on the surface of the coating, which were caused by the preferential dis-

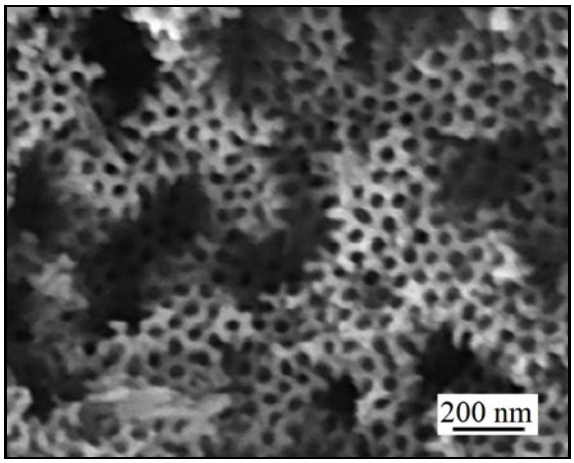

Fig 1. FE-SEM micrograph of the AHC surface obtainec from hard anodizing process.

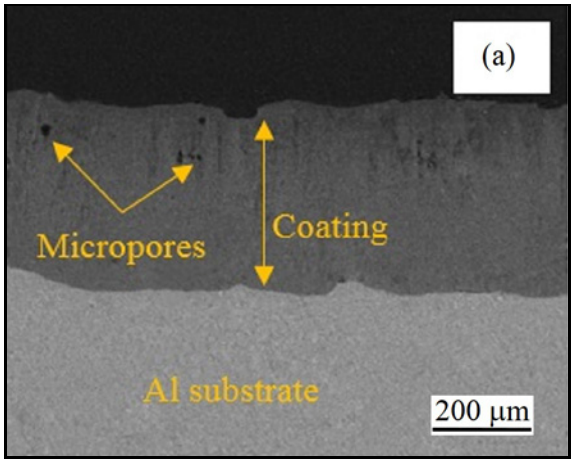

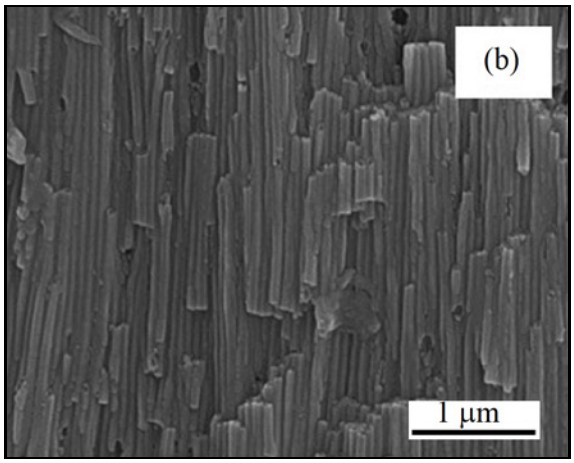

Fig. 2. FE-SEM micrographs of the (a) cross section and (b) fracture surface of the AHC sample.

solution of coarse intermetallic compounds into the electrolyte during anodizing [20]. Figure 2b shows the cross-section of the AHC with the pores parallel to each other and perpendicular to the surface of the coating.

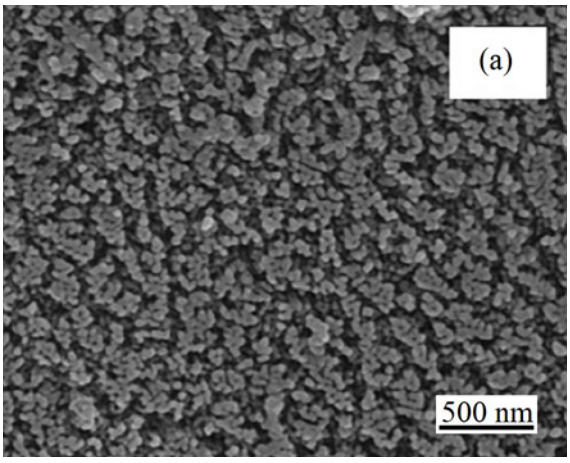

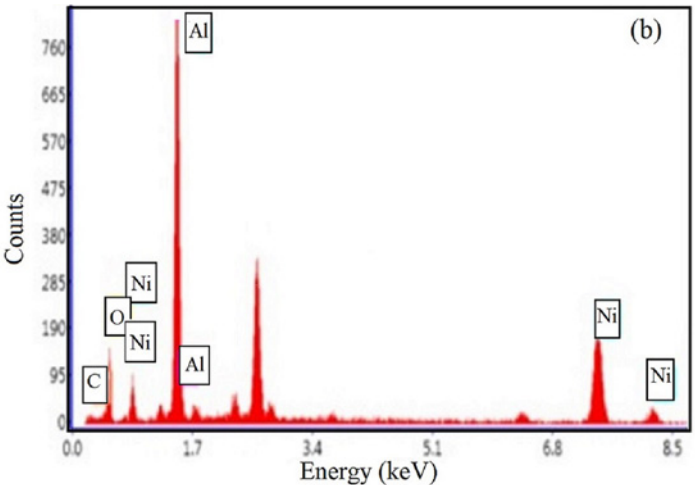

Fig. 3. (a) FE-SEM micrograph and (b) EDS analysis of the AHC + Ni composite coating surface.

3.2. Microstructure of the AHC + Ni composite coating

Figure 3 shows the FE-SEM and EDS analysis of the top surface of the AHC + Ni composite coating. EDS analysis (Fig. 3b) confirmed the presence of Ni precipitates on the surface of the AHC + Ni composite coating. The pores seem to be filled with Ni, and the mean diameter of Ni precipitates is similar to that of AHC pores (Fig. 1).

3.3. Microstructure of the AHC + Ni/Gr composite coatings

Top surface FE-SEM micrographs of AHC + Ni/Gr composite coatings obtained after different plating times are presented in Fig. 4. As can be seen, Ni precipitates have filled the pores and protruded from the top surface of the anodic oxide layer. These

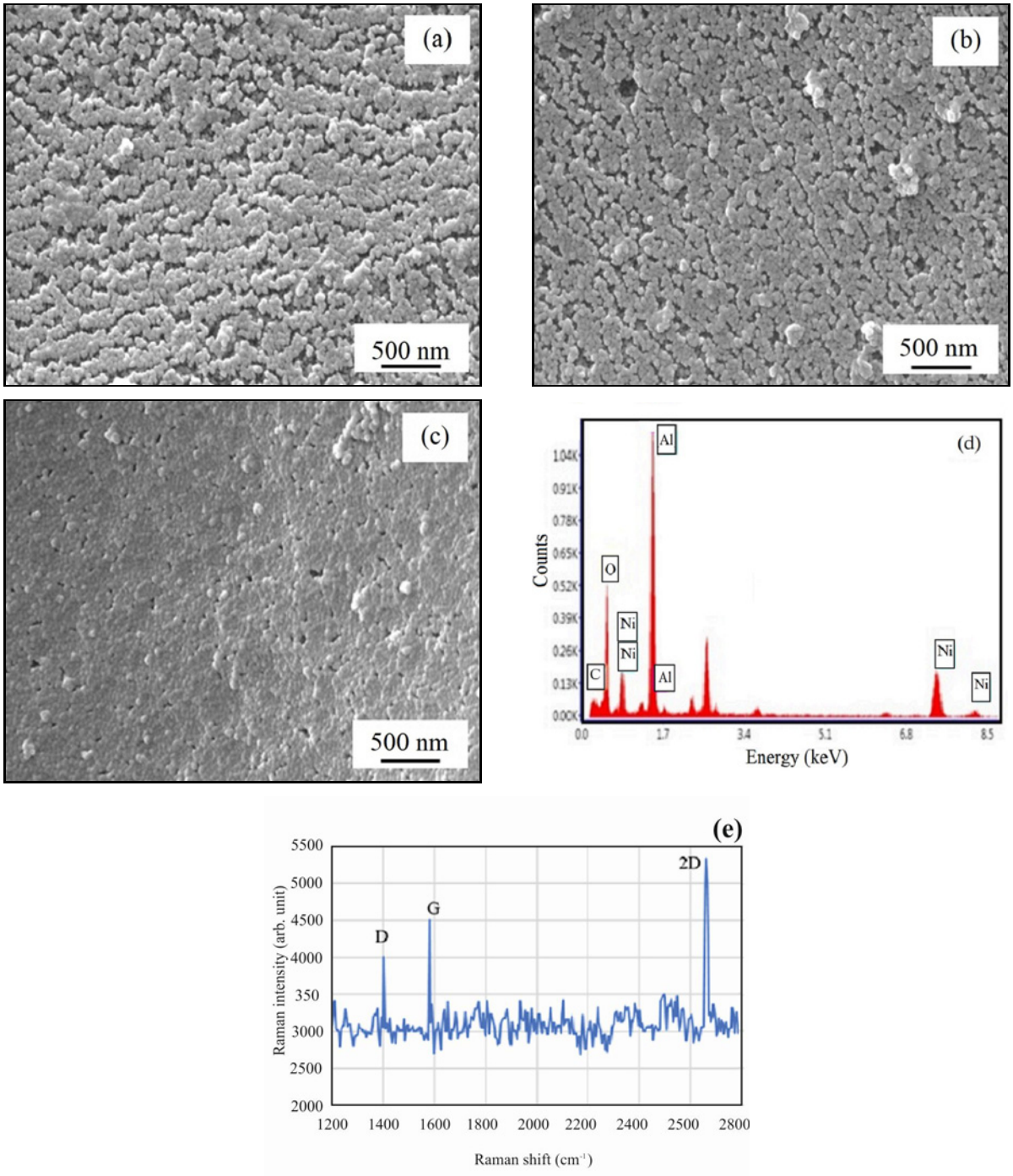

Fig. 4. FESEM micrographs of the AHC + Ni/Gr composite coatings' surface after different plating times (minutes): (a) AHC + Ni/Gr (10 min), (b) AHC + Ni/Gr (15 min), and (c) AHC + Ni/Gr (20 min), (d) EDS analysis, and (e) Raman spectra of the AHC + Ni/Gr (10 min) composite coating surface.

protrusions can be beneficial, as AHC has high surface roughness, and these protrusions can reduce steel pin/AHC contact during sliding tests [9]. It can also be seen that by increasing the plating time, the protrusions merge more together; thus, AHC + Ni (20) shows more coherency in protrusions.

Figure 5 shows the current-deposition time graph obtained from the Ni/Gr solution. This curve can be divided into four stages. In the pre-growth stage, a sudden current drop occurs as a result of applying the potential which the nucleation process starts at the pore bottoms. Valizadeh et al. pointed out that this sudden drop in the current is related to the mass transmission limitation [21]. The second stage, in which the metal particles grow in the pores, is characterized by a slight increase in the current. In the third stage,

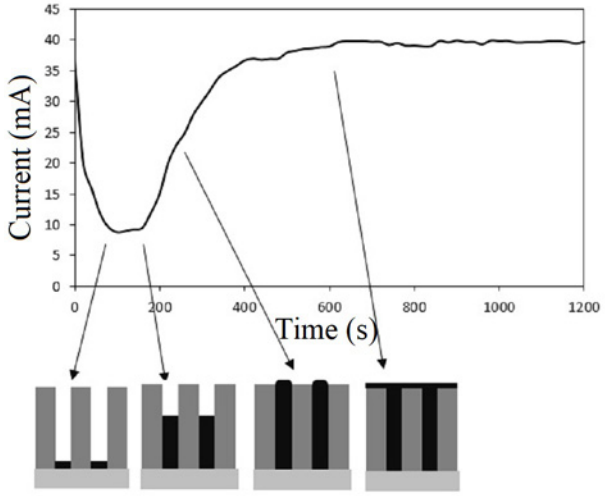

Fig. 5. Variations of current with respect to plating time for the AHC + Ni/Gr composite coating.

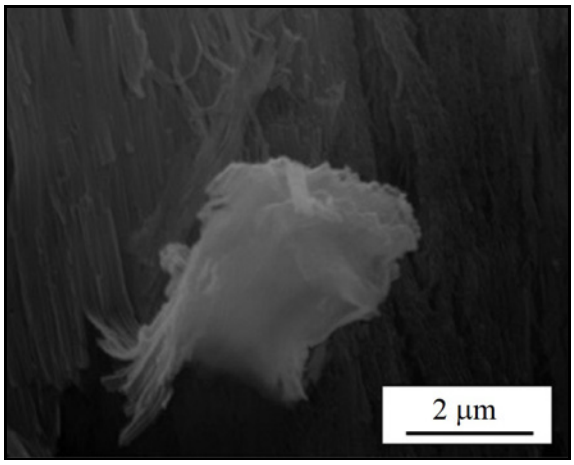

Fig. 6. FE-SEM micrographs of the fracture surface of AHC + Ni/Gr (10 min) composite coating showing a protruded graphene nanosheet.

pores are filled, and the current increases with a large gradient versus time. In the final stage, hemispherical caps originating from each nanowire expand and form a coherent planar layer on the surface. The current is stabilized as the active surface area approaches the geometric surface area of the substrate [22]. As shown in Fig. 5, the current has reached a steady value after 10 min (600 s), the time after which hemispherical caps start to form the coherent planar layer.

EDS analysis of the surface of AHC + Ni/Gr (10) composite coating, shown in Fig. 4d, confirms the presence of Ni and graphene in the coating. Figure 4e shows the Raman spectra of AHC + Ni/Gr (10) composite coating. The G, D, and 2D peaks were observed at 1402, 1580, and 2660 cm^{-1}, confirming the presence of graphene in the coating.

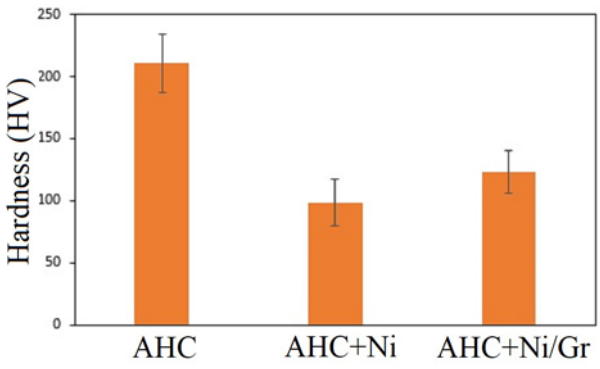

Fig. 7. The micro-hardness of the AHC, AHC + Ni, and AHC + Ni/Gr (20 min) coatings.

The fracture surface of AHC+Ni/Gr (10) is shown in Fig. 6. As can be seen, the graphene nanosheet protruded from the fractured surface of the coating. This can be considered as an evidence of the codeposition of graphene nanosheets and Ni into the pores of the AHC. During the electroplating process using an external electric field, the movement of Ni ions, which have a positive charge, is accelerated toward the bottom of the pores, which have a negative charge. Since the surface of the graphene nanosheet exhibits a negative charge, it can be adsorbed by Ni ions. The graphene nanosheet can be folded and wrinkled and enter the pores with the aid of moving Ni ions. Finally, Ni ions are reduced at the bottom of the pores and deposit as Ni precipitates containing graphene nanosheet.

3.4. Hardness

The average hardness values of the AHC, AHC + Ni, and AHC + Ni/Gr coatings are presented in Fig. 7. The hardness values of AHC and AHC + Ni coatings are 268 ± 45 and 100 ± 37 HV, respectively. The presence of Ni precipitates in AHC pores decreased the hardness of the coating. However, the hardness of the AHC + Ni/Gr (20) composite coating is 160 ± 34 HV, about 60 % higher than that of the AHC + Ni composite coating. A possible cause for this can be that graphene nanosheets in plating solution increase the nucleation sites for Ni ion reduction, and result in the refinement of the Ni matrix grain structure, which can increase hardness. The mechanical strength of graphene (130 GPa) can also play a vital role in enhancing the micro-hardness of the AHC + Ni/Gr composite coating. These results indicate that simultaneous precipitation of Ni and graphene nanosheets results in the higher hardness of AHC + Ni/Gr composite coating in comparison to AHC + Ni composite coating, and it compensates for the hardness reduction caused by Ni precipitation.

Table 2. Surface roughness parameter values for the AHC, AHC + Ni, and AHC + Ni/Gr coatings after different plating times

Coatings	Average surface roughness R_a (μm)	Root mean square roughness R_q (μm)	Average maximum height of the profile R_z (μm)	Kurtosis R_{ku}(dimensionless)
AHC	1.15	1.53	12.67	8.67
AHC + Ni	0.56	0.81	7.62	7.32
AHC + Ni/Gr (10)	2.76	3.48	21.29	11.06
AHC + Ni/Gr (15)	2.12	2.77	19.11	9.01
AHC + Ni/Gr (20)	1.90	2.49	18.09	10.85

Table 3. Wear rate and wear loss of pin, and average friction coefficient of the AHC, AHC + Ni, and AHC + Ni/Gr coating

Coatings	Wear rate $\times 10^{-6}$ ($mm^3\ N^{-1}\ m^{-1}$)	Weight loss of steel pin (mg)	Friction coefficient
AHC	11.8	0.6	1.10
AHC + Ni	13.3	0.3	1.02
AHC + Ni/Gr (10)	0.95	0.1	0.97
AHC + Ni/Gr (15)	1.6	0.5	0.88
AHC + Ni/Gr (20)	3	0.2	1.03

3.5. Roughness

Surface roughness parameters of the AHC, AHC + Ni, and AHC + Ni/Gr (20) coatings are presented in Table 2. As can be seen, when pores of AHC are filled with Ni precipitates, the surface roughness is considerably reduced. Codeposition of graphene resulted in increasing the surface roughness of the deposited layers since graphene codeposited both between the Ni grains and the surface of the coatings [18]. It is also clear that with an increase in the plating time, the surface roughness of the AHC + Ni/Gr coatings has reduced. This can be explained by the increase in the coherency of the precipitates with an increase in the plating time.

3.6. Wear and friction results

Table 3 shows the wear rate, weight loss of pin, and average friction coefficient of AHC, AHC + Ni, and AHC + Ni/Gr coatings. The wear rate of AHC + Ni composite coating seems to be higher than that of AHC. The presence of Ni precipitates in anodic oxide coating results in the reduction of the hardness and wear resistance of the coating. However, AHC + Ni/Gr composite coating showed a significantly lower wear rate compared to AHC and AHC + Ni coatings. It can be inferred that the graphene nanosheets in the coating are responsible for this difference in wear properties since they can be detached from the Ni matrix, act as a solid lubricant, bear the Ni matrix stress, and thus, decrease the shear force between the contact surfaces [16].

The weight loss of the steel pin against the AHC + Ni coating was 0.3 mg, about two times lower than that against AHC, due to the presence of Ni precipitations in the pores of the anodic oxide coating. At the beginning of friction, Ni precipitations can prevent direct contact between the steel pin and anodic oxide coating, and thus, the wear of the steel pin is reduced. In the main stage of friction, the height of Ni precipitates reaches the bulge of the anodic oxide coating, and the wear of the steel pin is increased. This increase in wear is caused by the direct contact between the steel pin and the bulges of the anodic oxide coating. However, at this stage of friction, the weight loss in the steel pin against the AHC + Ni coating is lower than against the AHC. The lowest weight loss of the steel pin was obtained against the AHC + Ni/Gr (10) composite coating.

Reduction in the friction coefficient of the AHC + Ni and AHC + Ni/Gr composite coatings compared to that of AHC is associated with the presence of Ni precipitations and graphene nanosheets with low shear strength. According to Table 3, AHC + Ni/Gr (15) composite coating exhibited the lowest friction coefficient. Figure 8 shows the wear tracks of AHC + Ni/Gr composite coatings obtained after different plating times. As can be seen, a tribo-layer is formed on the wear tracks of the coatings. AHC + Ni/Gr (15) composite coating shows a darker tribo-layer due to the higher thickness of this layer. The tribo-layer reduces the friction at the contact surface [23]. Hence,

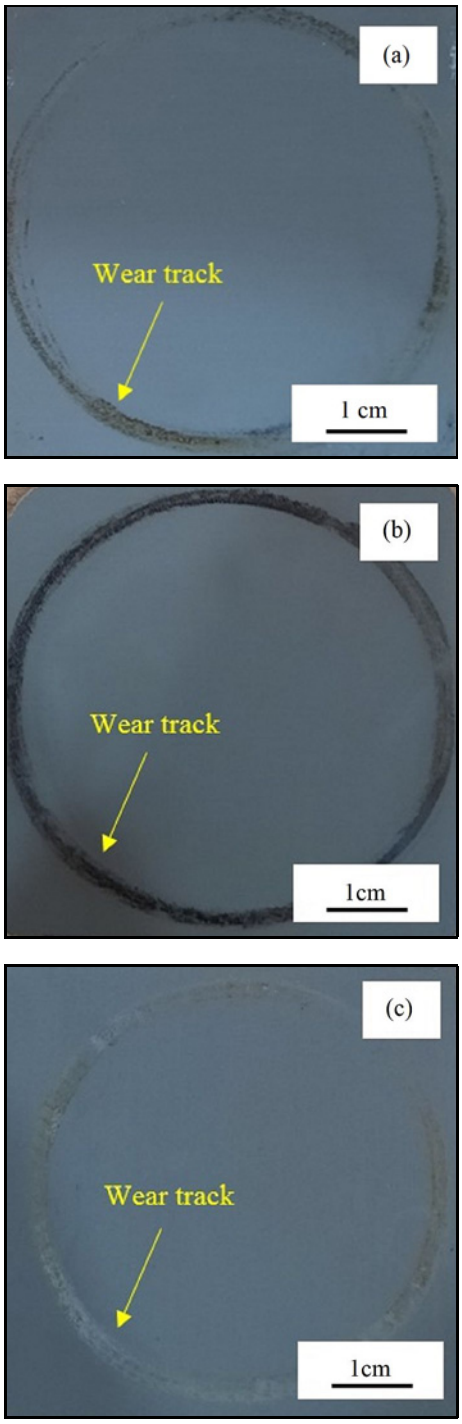

Fig. 8. SEM micrographs of wear tracks of the AHC + Ni/Gr composite coatings after different plating times: (a) AHC + Ni/Gr (10 min), (b) AHC + Ni/Gr (15 min), and (c) AHC + Ni/Gr (20 min).

the formation of a thick tribo-layer is one of the reasons for the reduction in the friction coefficient. Moreover, the presence of Ni precipitations and graphene nanosheets, with low shear strength, in AHC + Ni and AHC + Ni/Gr composite coatings can be considered as the main reason for the lower friction coefficient of these coatings in comparison to the AHC. Siddaiah et al. [24] investigated the effect of surface energy on the tribological behavior of pure nickel coatings and Ni/Gr composite coatings. The authors reported that the Ni/Gr composite coating exhibited low surface energy, which is suggestive of weak adhesive forces between the wear particles and the surface. Moreover, graphene nanosheets, as a solid lubricant, facilitate shearing and reduce the friction coefficient.

Figure 9 shows the variations in the friction coefficients of the AHC, AHC + Ni, and AHC + Ni/Gr coatings versus the sliding distance. As can be seen, the friction coefficient of the AHC increased in the first 80 m of sliding distance and then remained constant. It can be related to the formation of a tribo-layer [25]. Figure 10a shows the EDS analysis of the wear track of AHC, which is composed of Fe and Cr transferred from the steel pin, and Al, S, and O, which are the main chemical elements of the oxide layer of AHC. The formation of the tribo-layer can be affected by factors such as sliding speed and normal load. High sliding speed and high normal load generate more heat at the friction contact, and, thus, accelerate the oxidation phenomena and the formation of tribo-layer [26]. By increasing the sliding distance, parts of the tribo-layer are detached from the surface due to delamination [27], which is confirmed by the observation of Fe and Cr particles in the EDS analysis of wear debris (Fig. 10b). The carbon peak observed in the EDS analysis is most likely related to the graphite paper used to collect the wear debris.

Figure 9b shows the variations of the friction coefficient of AHC + Ni composite coating versus sliding distance. The surface roughness of this coating is lower than that of AHC (Table 2). Furthermore, the friction coefficient of AHC + Ni composite coating reached the steady-state condition at a shorter sliding distance.

Figures 9c–e show the variations of friction coefficient versus sliding distance for AHC + Ni/Gr composite coatings obtained after different plating times. As can be seen, there is less fluctuation in the friction coefficient of AHC + Ni/Gr (20) composite coating at the beginning of sliding in comparison with AHC + Ni/Gr (10) and AHC + Ni/Gr (15) composite coatings. This can be related to the lower surface roughness of AHC + Ni/Gr (20) composite coating compared to AHC + Ni/Gr (10) and AHC + Ni/Gr (15) coatings (Table 2). According to Figs. 9c–e, with an increase in the plating time, the sliding distance required to attain steady-state friction has reduced. In other words, the sliding distance of the steady-state friction coefficient tends to become shorter with the decreasing of surface roughness parameters (R_a, R_q) [28]. Steady-state friction in AHC + Ni/Gr composite coatings can be attributed to the formation of a tribo-layer consisting of graphene nanosheets and a mixture

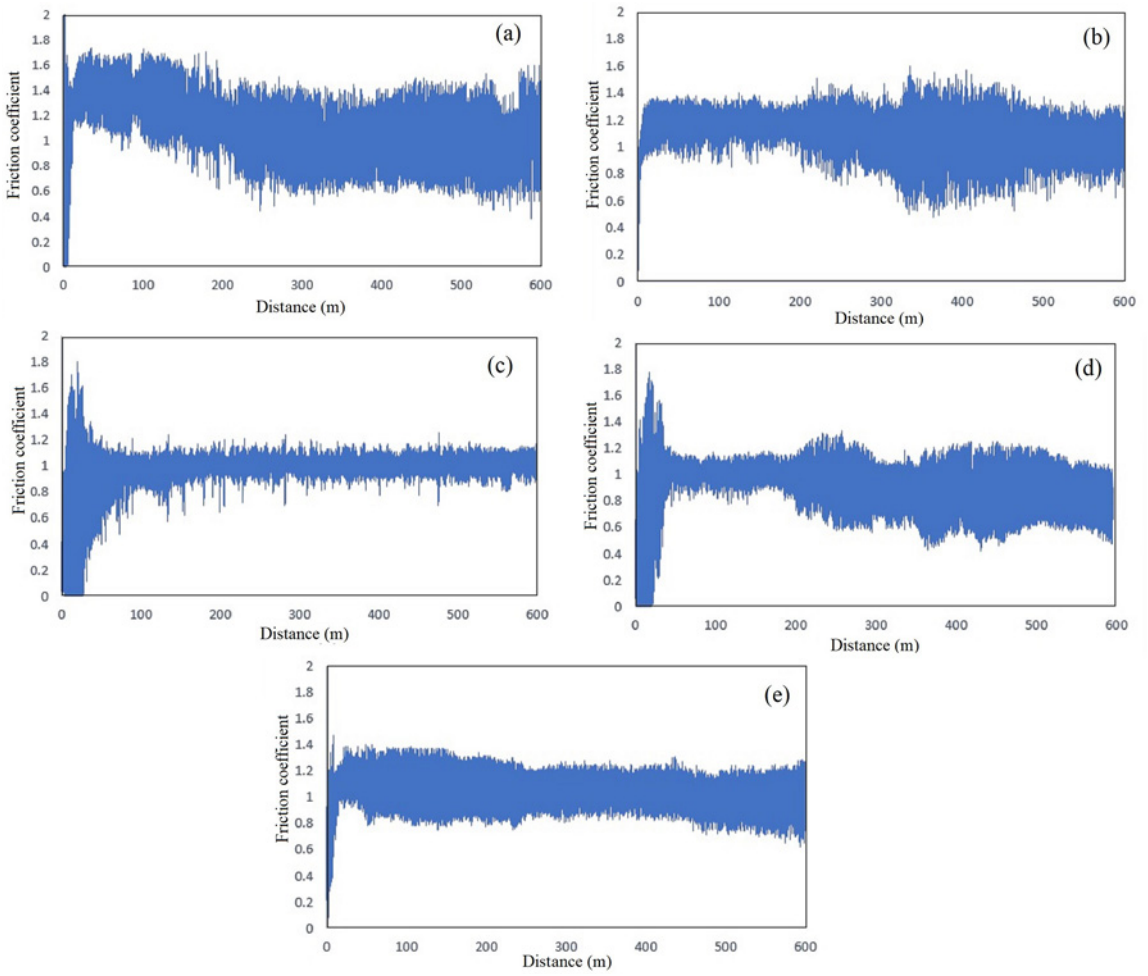

Fig. 9. Friction coefficient variation versus sliding distance for (a) AHC, (b) AHC + Ni, (c) AHC + Ni/Gr (10 min), (d) AHC + Ni/Gr (15 min), and (e) AHC + Ni/Gr (20 min).

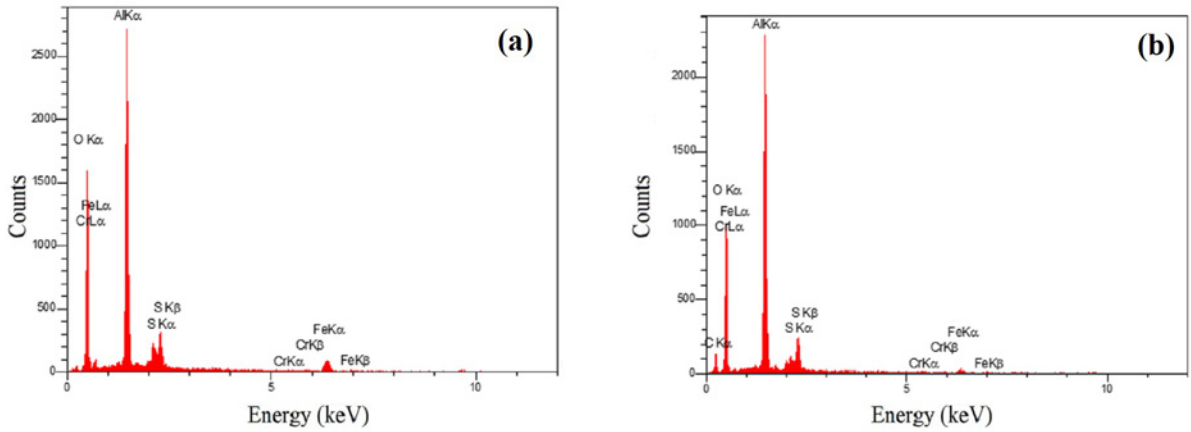

Fig. 10. EDS analysis of the (a) wear track and (b) wear debris after wear test of the AHC against the steel pin.

of fractured aluminum oxide particles, nickel particles, and iron particles from the steel pin [23].

Two different components are believed to control the friction coefficient: (a) an adhesive force acting at the real contact surface and (b) a deformation force acting the ploughing of the asperities of a harder surface in a softer metal surface. Therefore, the friction coefficient can be written as follows [29]:

$$\mu = \mu_a + \mu_p, \tag{1}$$

Table 4. Stick-slip parameters of different coatings

Stick-slip parameters	AHC	AHC + Ni	AHC + Ni/Gr (10)	AHC + Ni/Gr (15)	AHC + Ni/Gr (20)
A	1	0.75	0.3	0.8	0.4
F_s	2.24	1.27	1.8	1.8	1.47
F_k	1.10	1.02	0.97	0.88	1.03

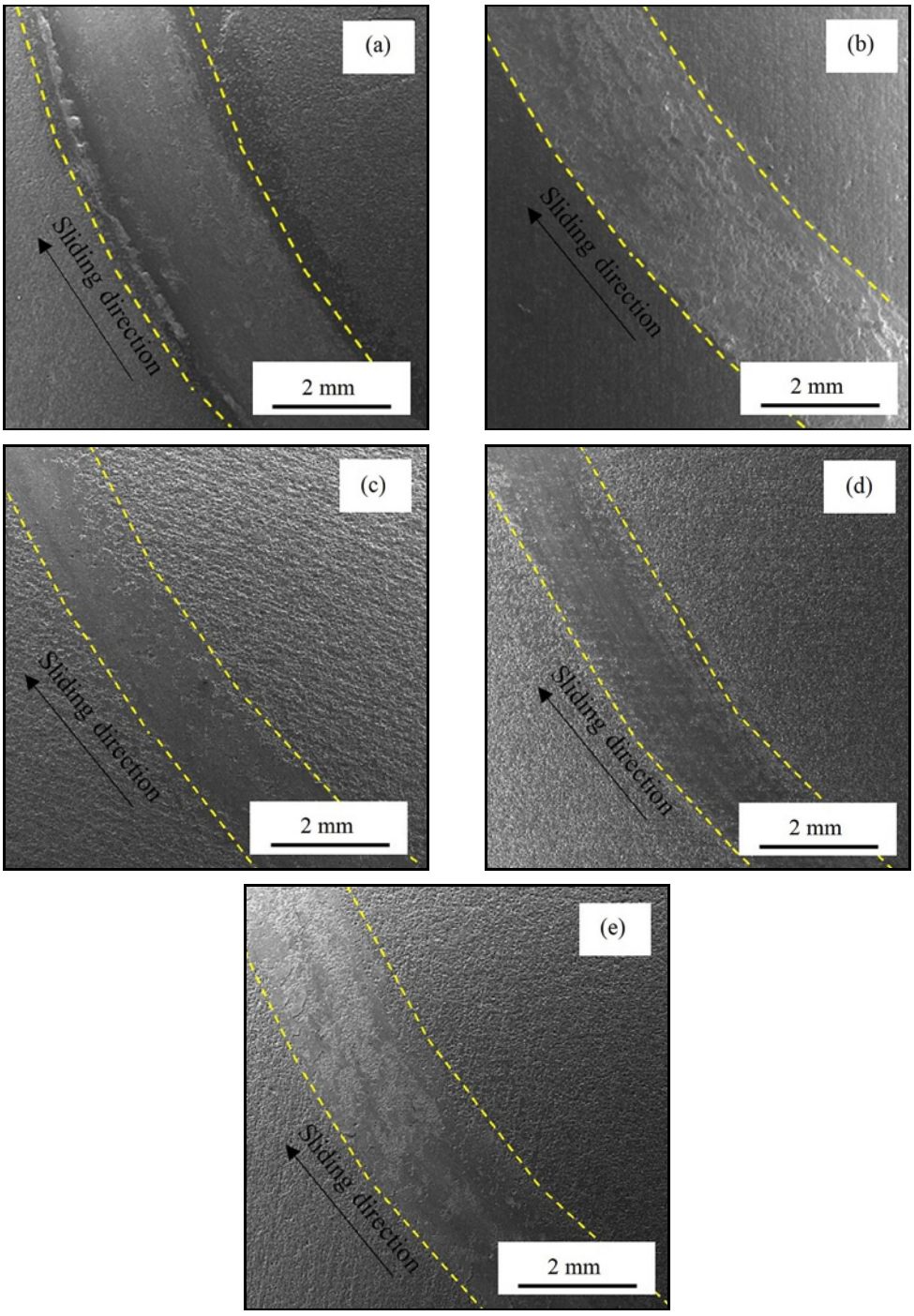

Fig. 11. Low magnification SEM morphologies of the wear tracks of (a) AHC, (b) AHC + Ni, (c) AHC + Ni/Gr (10 min), (d) AHC + Ni/Gr (15 min), and (e) AHC + Ni/Gr (20 min) coatings.

where μ_a is the adhesive component of the materials, and μ_p is the ploughing component that is related to the texture of the tribo-surfaces in contact.

In Fig. 9, there are some fluctuations in the fric-

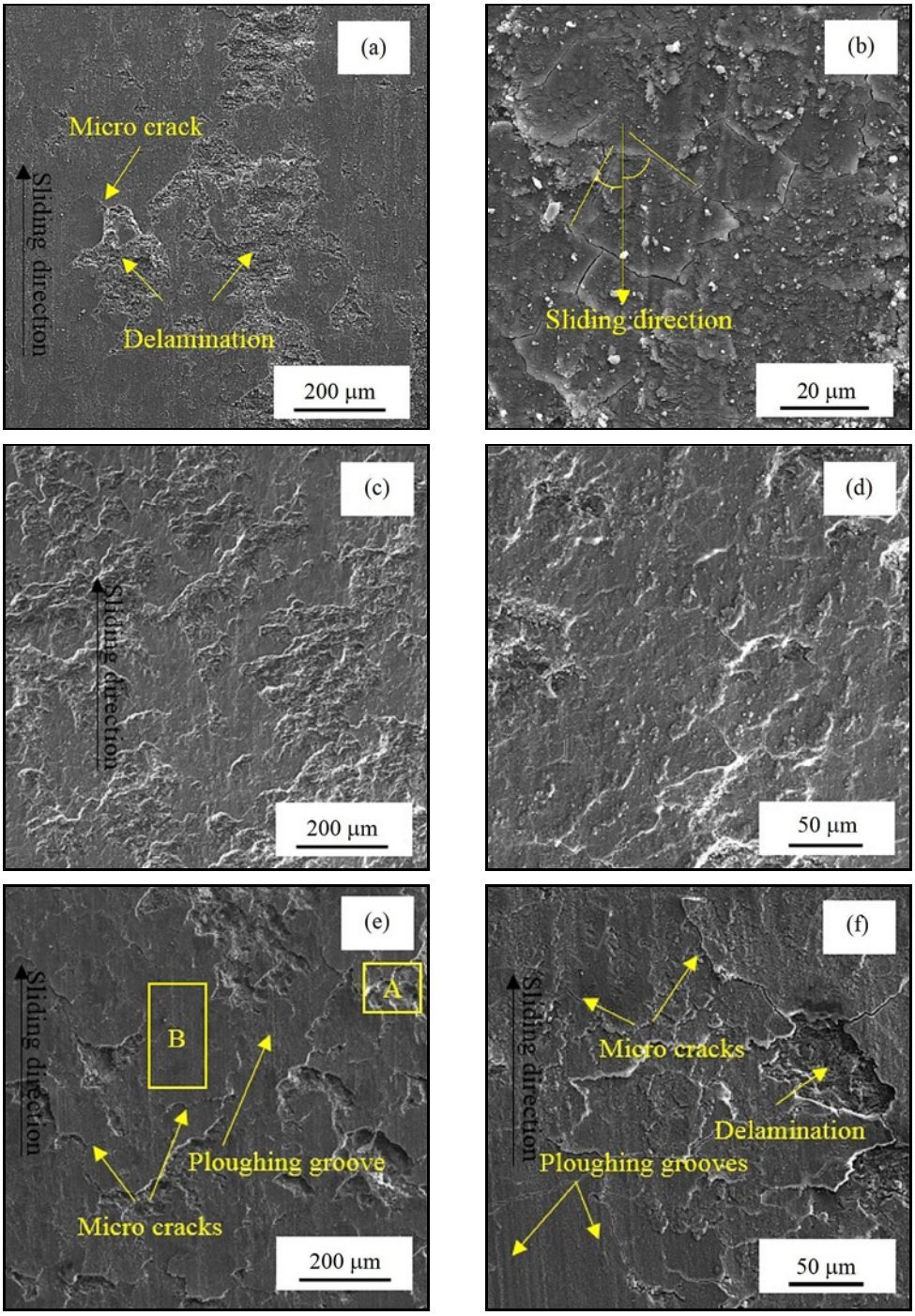

Fig. 12a–f. Enlarged SEM morphologies of wear tracks of (a), (b) AHC; (c), (d) AHC + Ni; (e), (f) AHC + Ni/Gr (10 min).

tion coefficient during the wear test. Manzez et al. [29] attributed these fluctuations to the stick-slip effect related to the friction process and the adhesive component. The amplitude of these fluctuations is not affected by surface roughness parameters (R_a and R_q), but is influenced by the ploughing component of the friction. Under dry sliding conditions, the ploughing component is mostly affected by the R_{ku} parameter [29]. Higher values of the R_{ku} parameter cause lower stress, and the corresponding ploughing component of friction results in mild shear failure and lower material transfer. Therefore, the stick-slip amplitude of fluctuations can be explained by the R_{ku} parameter. The amplitude of the friction coefficient fluctuations of AHC + Ni/Gr (15) composite coating with the lowest R_{ku} (Table 2) was higher than that of AHC + Ni/Gr (10) and AHC + Ni/Gr (20) composite coatings. Three parameters have been derived to explain the stick-slip phenomenon, namely amplitude of fluctuations, static friction coefficient (F_s), which is

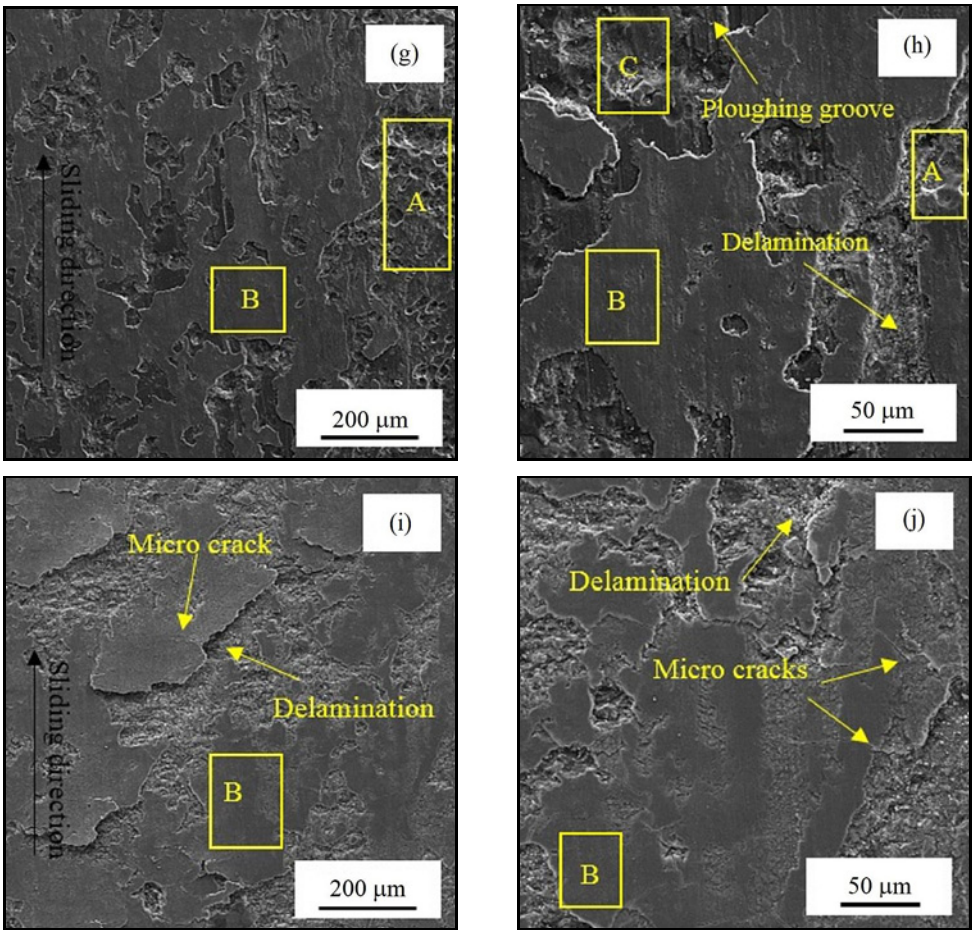

Fig. 12g–j. Enlarged SEM morphologies of wear tracks of (g), (h) AHC + Ni/Gr (15 min); and (i), (j) AHC + Ni/Gr (20 min) coatings.

the coefficient at the beginning of friction, and kinetic friction coefficient (F_k), which is the average value at steady-state [30]. These parameters have been listed in Table 4 for all the different coatings. AHC showed higher stick-slip parameters due to its rough surface and the existence of particles transferred from the steel pin. In AHC + Ni/Gr composite coatings, the simultaneous presence of Ni precipitates with low shear strength and graphene nanosheets with good lubrication properties resulted in easier shearing between the contact surfaces. Thus, the stick-slip parameters of these coatings were lower than those of AHC and AHC + Ni coatings.

Figure 11 shows the SEM images obtained from the worn surfaces of AHC, AHC + Ni, and AHC + Ni/Gr coatings at low magnification. As can be seen, the width of the wear track on the AHC is larger than those formed on the surface of AHC + Ni and AHC + Ni/Gr coatings. No trace of plastic deformation could be detected on the worn surface of AHC, which is related to the high hardness and brittleness of this coating. However, as depicted in Fig. 11b, signs of plastic deformation were found in the wear track of the AHC + Ni coating. AHC + Ni/Gr composite coatings exhibited narrower wear tracks with fewer regions showing plastic deformation that can be explained by the higher hardness of these coatings in comparison with AHC + Ni composite coating. Furthermore, in these coatings, graphene nanosheets can act as a load-bearing solid lubricant [31]. It can also be seen in Figs. 11c–e that the width of the wear track on the AHC + Ni/Gr (20) is larger than on AHC + Ni/Gr (10) and AHC + Ni/Gr (15), which is related to the lower wear resistance of this coating.

Figure 12 shows the high-magnification SEM micrographs obtained from the wear tracks of AHC, AHC + Ni, and AHC + Ni/Gr coatings. Traces of delamination as well as microcracks can be observed in Fig. 12a. All cracks have identical angles regarding the sliding direction (Fig. 12b). This means that cracks are created together on both sliding sides along the wear tracks [27]. Some low-depth grooves parallel to the wear direction can also be seen in Fig. 12b. The appearance of cracks along with zones showing delamination and grooves means that abrasion and delamination are the main wear mechanisms.

Exfoliation in Figs. 12c,d confirms that the main wear mechanism in AHC + Ni coating is fatigue

wear. As shown in Fig. 2a, micropores in anodic oxide coating formed crack sources that expanded and created exfoliation under periodically applied load during wear testing [32].

Figures 12e,j show the SEM micrographs obtained from the wear tracks of AHC + Ni/Gr coatings obtained after different plating times. In the first stages of wear, the pressure applied onto the surface is high; therefore, higher asperities on the surface can come in contact with the steel pin and be crushed. These zones are typically like the area marked as "B" in Fig. 12e. Regions like "A" are probably areas of lower height on the surface that were not in contact with the steel pin. In Fig. 12f, low-depth ploughing grooves, flakes, and some microcracks can be seen in the wear track. Graphene nanosheets in the AHC + Ni/Gr composite coatings can cause the diminishing of delamination and abrasive wear mechanisms. This can be related to the higher hardness of AHC + Ni/Gr (10) composite coating and the lubrication property of graphene nanosheets. Thus, the codeposition of graphene nanosheets and Ni in the anodic oxide coating seems to change the wear mechanism from fatigue to slight abrasion and delamination wear.

As shown in Figs. 12g,h the surface of the coating obtained after a higher plating time (15 min), marked as "B", exhibited more non-uniformity. As presented in Table 2, AHC + Ni/Gr (15) coating possessed a lower R_{ku} than AHC + Ni/Gr (10). When R_{ku} decreases, the contact surface is reduced; this means that in the first stages of the wear, in which the applied stress is high, the number of contact points between the coating surface and the steel pin will be reduced. The tribo-layer is created on the contact surface, and for the AHC + Ni/Gr (15) coating, it is non-uniform. This tribo-layer can increase the wear resistance of the coating; hence, the wear rate of AHC + Ni/Gr (15) coating is higher than that of AHC + Ni/Gr (10) (Table 3). The height of regions marked as "C" in Fig. 12h is less and more relative to areas "B" and "A", respectively. Regions denoted as "C" come in contact with the steel pin after areas "B". Therefore, these regions were exposed to lower pressures compared to areas "B". In addition, microcracks and flakes are evident on the wear track, which indicates that slight delamination and abrasion are the dominant wear mechanisms in this coating. The coating obtained after the longest plating time (20 minutes) showed a different morphology on the wear track. According to Figs. 12i,j, this coating showed only areas "B" with flakes and microcracks, and zones with the characteristics of regions "A" and "C" could not be detected. Since the AHC + Ni/Gr (20) composite coating possessed lower surface roughness, more points on the surface of this coating might have been in contact with the steel pin during sliding wear. Accordingly, the higher wear rate of this coating compared to the other two coatings is expectable (Table 3).

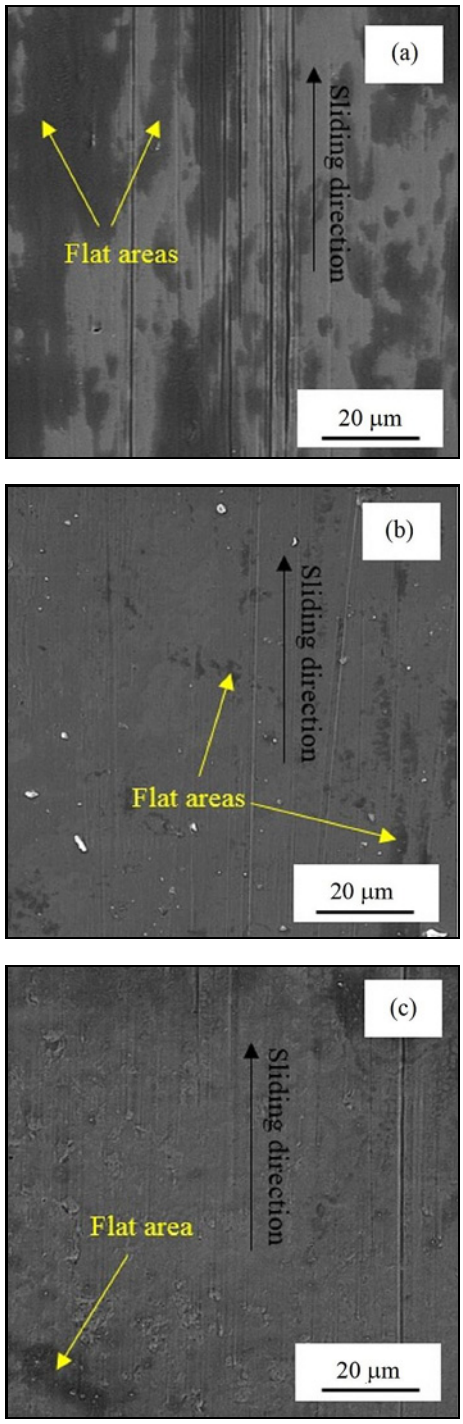

Fig. 13. SEM morphologies of the worn steel pin surface after sliding in contact with (a) AHC, (b) AHC + Ni, and (c) AHC + Ni/Gr (10 min) coatings.

Figure 13 shows the SEM micrographs of the worn steel pin in contact with AHC, AHC + Ni, and AHC + Ni/Gr (10) coatings. Significant flat areas have been created on the worn surface of the steel pin; this con-

firms the materials' transfer from the steel pin surface to the AHC coating surface (Fig. 13a). In addition, scratches created due to the asperities of AHC coating can also be seen. The flat areas created on the worn surface of AHC + Ni and AHC + Ni/Gr (10) coatings (Figs. 13b,c) imply the lower wear of the steel pin against these coatings.

4. Conclusions

AHC + Ni/Gr composite coating was successfully produced by electroplating of anodic hard coating. AHC + Ni/Gr composite coating exhibited 160 ± 34 HV micro-hardness, which was 60 percent higher than that of AHC + Ni composite coating (100 ± 37 HV). With increasing the plating time, the roughness of the AHC + Ni/Gr coating surface was reduced, which was attributed to the higher coherency of the precipitates obtained after a longer plating time. The simultaneous presence of Ni and graphene resulted in lower stick-slip parameters in AHC + Ni/Gr coating. AHC + Ni/Gr coating possessed lower wear rate, friction coefficient, and weight loss against steel pin in comparison with AHC and AHC + Ni coatings. AHC + Ni/Gr composite coating obtained with 10 min plating time showed the lowest wear rate and weight loss on the steel pin. The steel pin showed the highest weight loss when worn against AHC. The dominant wear mechanism of AHC + Ni coating was suggested to be fatigue wear, which changed to slight abrasive and delamination mechanisms in AHC + Ni/Gr composite coatings.

Acknowledgements

The present research was supported by the Shahid Chamran University of Ahvaz under grant number SCUEM99223.

References

[1] M. M. Lohrengel, Thin anodic oxide layer on aluminum and other valve metal: high field regime, Mater. Sci. Eng. 11 (1993) 243–294. https://doi.org/10.1016/0927-796X(93)90005-N

[2] F. Debuyck, M. Moors, A. P. Vanpeteghem, The influence of the anodization temperature and voltage on the porosity of the anodization layer on aluminum, Mater. Chem. Phys. 36 (1993) 146–149. https://doi.org/10.1016/0254-0584(93)90023- F

[3] V. López, J. A. González, E. Otero, E. Escudero, M. Morcillo, Atmospheric corrosion of bare and anodized aluminum in a wide range of environmental conditions, Part II: Electrochemical responses, Surf. Coat. Technol. 153 (2002) 235–244. https://doi.org/10.1016/S0257-8972(01)01681-4

[4] F. Snogan, C. Blanc, G. Mankowski, N. Pébère, Characterization of sealed anodic films on 7050 T74 and 2214 T6 aluminum alloys, Surf. Coat. Technol. 154 (2002) 94–103. https://doi.org/10.1016/S0257-8972(01)01717-0

[5] A. Rajendra, B. J. Parmar, A. K. Sharma, H. Bhojraj, M. M. Nayak, K. Rajanna, Hard anodization of aluminum and its application to sensorics, Surf. Eng. 21 (2005) 193–197. https://doi.org/10.1179/174329405X50000

[6] L. Chen, Z. Liu, Q. Shen, Enhancing tribological performance by anodizing micro-textured surfaces with nano-MoS_2 coatings prepared on aluminum-silicon alloys, Tribol. Int. 122 (2018) 84–95. https://doi.org/10.1016/j.triboint.2018.02.039

[7] Y. Zhao, M. Chen, W. Liu, X. Liu, Q. Xue, Preparation and self-lubrication treatment of ordered porous anodic alumina film, Mater. Chem. Phys. 82 (2003) 370–374. https://doi.org/10.1016/S0254-0584(03)00265-7

[8] W. Zhang, D. Zhang, Y. Le, L. Li, B. Ou, Fabrication of surface self-lubricating composites of aluminum alloy, Appl. Surf. Sci. 255 (2008) 2671–2674. https://doi.org/10.1016/j.apsusc.2008.07.209

[9] A. Posmyk, Co-deposited composite coatings with a ceramic matrix destined for sliding pairs, Surf. Coat. Technol. 206 (2012) 3342–3349. https://doi.org/10.1016/j.surfcoat. 2012.01.004

[10] W. Gumowska, I. Dobosz, M. Uhlemann, J. Koza, Al_2O_3-Fe composites obtained by the electrochemical method, Arch. Metall. Mater. 54 (2009) 1119-1133.

[11] A. Posmyk, Forming tribological properties of surface layers on aluminium materials, Publisher of Silesian University of Technology, Gliwice (2002).

[12] A. Posmyk, Influence of material properties on the wear of composite coatings, Wear 254 (2003) 399–407. https://doi.org/10.1016/S0043-1648(03)00130-3

[13] A. Posmyk, Composite coating with ceramic matrix including Ni nanowires, Surf. Eng. 29 (2013) 171–176. https://doi.org/10.1179/1743294412Y.0000000109

[14] Z. Ren, N. Meng, K. Shehzad, Y. Xu, S. Qu, B. Yu, J. K. Luo, Mechanical properties of nickel-graphene composites synthesized by electrochemical deposition, Nanotechnology 26 (2015) 065706. https://doi.org/10.1088/0957-4484/26/6/065706

[15] Y. Dong, W. Sun, X. Liu, M. Ma, Y. Zhang, Y. Liu, Electrophoretic deposition of graphene and microstructure and friction behavior of Ni-graphene composite coatings, Adv. Eng. Mater. 21 (2019) 1900327. https://doi.org/10.1002/adem.201900327

[16] O. Özkan, H. Mindivan, An electroplating method of nickel–graphene composite coatings on Ti-6Al-4V alloy, Bilgesci. 2 (2018) 47–52. https://doi.org/10.30516/bilgesci.476442

[17] H. Zhang, N. Zhang, F. Fang, Fabrication of high-performance nickel/graphene oxide composite coatings using ultrasonic-assisted electroplating, Ultrason. Sonochem. 62 (2020) 104858. https://doi.org/10.1016/j.ultsonch.2019.104858

[18] H. Algul, M. Tokur, S. Ozcan, M. Uysal, T. Cetinkaya, H. Akbulut, A. Alp, The effect of graphene content and sliding speed on the wear mechanism of nickel–graphene nanocomposites, Appl. Surf. Sci. 359 (2015) 340–348. https://doi.org/10.1016/j.apsusc.2015.10.139

[19] A. Posmyk, H. Wistuba, Composite layers with ceramic matrix modified with glassy carbon destined for

oil-less sliding pairings, Arch. Metall. Mater. 56 (2011) 909–9017. https://doi.org/10.2478/v10172-011-0100-2
[20] P. Kwolek, K. Krupa, A. Obłój, P. Kocurek, M. Wierzbińska, J. Sieniawski, Tribological properties of the oxide coatings produced onto 6061-T6 aluminum alloy in the hard anodizing process, J. Mater. Eng. Perform. 27 (2018) 3268–3275. https://doi.org/10.1007/s11665-018-3421-8
[21] S. Valizadeh, J. M. George, P. Leisner, L. Hultman, Electrochemical synthesis of Ag/Co multilayered nanowires in porous polycarbonate membranes, Thin Solid Films 402 (2002) 262–271. https://doi.org/10.1016/S0040-6090(01)01674-1
[22] C. Frantz, C. Vichery, J. Zechner, D. Frey, G. Bürki, H. Cebeci, J. Michler, L. Philippe, Pulse electroplating of adherent nickel coatings onto anodized aluminum surfaces, Appl. Surf. Sci. 330 (2015) 39–47. https://doi.org/10.1016/j.apsusc.2014.12.091
[23] A. R. Riahi, A. T. Alpas, The role of tribo-layers on the sliding wear behavior of graphitic aluminum matrix composites, Wear 251 (2001) 1396–1407. https://doi.org/10.1016/S0043-1648(01)00796-7
[24] A. Siddaiah, P. Kumar, A. Henderson, M. Misra, P. L. Menezes, Surface energy and tribology of electrodeposited Ni and Ni–graphene coatings on steel, Lubricants 7 (2019) 87. https://doi.org/10.3390/lubricants7100087
[25] S. H. Mohitfar, S. Mahdavi, M. R. Etminanfar, J. Khalil-Allaf, Characteristics and tribological behavior of the hard anodized 6061-T6 Al alloy, J. Alloys Compd. 842 (2020) 155988. https://doi.org/10.1016/j.jallcom.2020.155988
[26] M. Guezmil, W. Bensalah, A. Khalladi, K. Elleuch, M. De-Petris Wery, H. F. Ayedi, Effect of test parameters on the friction behaviour of anodized aluminium alloy, Int. Sch. Res. Notices 2014 (2014) 795745. http://dx.doi.org/10.1155/2014/795745
[27] H. S. Kim, D. H. Kim, W. Lee, S. J. Cho, J. H. Hahn, H. S. Ahn, Tribological properties of nanoporous anodic aluminum oxide film, Surf. Coat. Technol. 205 (2019) 1431–1437. https://doi.org/10.1016/j.surfcoat.2010.07.056
[28] L. Chen, Z. Liu, B. Wang, Q. Song, Y. Wan, L. Chen, Surface characterization and tribological performance of anodizing micro-textured aluminum-silicon alloys, Materials 12 (2019) 1862. https://doi.org/10.3390/ma12111862
[29] P. L. Menezes, S. V. Kailas, Influence of surface texture and roughness parameters on friction and transfer layer formation during sliding of aluminum pin on steel plate, Wear 267 (2009) 1534–1549. https://doi.org/10.1016/j.wear.2009.06.003
[30] V. Perfilyev, A. Moshkovich, I. Lapsker, A. Laikhtman, L. Rapoport, The effect of vanadium content and temperature on stick-slip phenomena under friction of CrV(x)N coatings, Wear 307 (2013) 44–51. https://doi.org/10.1016/j.wear.2013.08.012
[31] L. Xu, R. Wang, M. Gen, L. Lu, G. Han, Preparation and properties of graphene/nickel composite coating based on textured surface of aluminum alloy, Materials 12 (2019) 3240. https://doi.org/10.3390/ma12193240
[32] Z. Li, S. Di, Preparation and properties of microarc oxidation self-lubricating composite coatings on aluminum alloy, Materials 7 (2017) 127. https://doi.org/10.3390/met7040127